Available online at www.sciencedirect.com
ScienceDirect
International Journal of Heat and Mass Transfer 50 (2007) 5139–5149
International Journal of HEAT and MASS TRANSFER
www.elsevier.com/locate/ijhmt

Effect of surface radiation on buoyant convection in vertical triangular cavities with variable aperture angles

Jaime Sieres [a,*], Antonio Campo [b], El Hassan Ridouane [b], José Fernández-Seara [a]

[a] Área de Máquinas y Motores Térmicos, E.T.S. de Ingenieros Industriales, Universidad de Vigo, Campus Lagoas-Marcosende, 36310 Vigo, Spain
[b] Department of Mechanical Engineering, The University of Vermont, Burlington, VT 05405, USA

Received 28 November 2006; received in revised form 9 July 2007
Available online 28 August 2007

Abstract

The present investigation deals with the numerical computation of laminar natural convection with and without surface-to-surface radiation in a class of right-angled triangular cavities filled with air. The vertical walls are uniformly heated and the inclined walls are uniformly cooled while the upper connecting walls are adiabatic. The aperture angle φ located at the lower vertex of the triangular cavities between the vertical and the inclined walls identifies the shape of each cavity. This kind of cavity finds application in the miniaturization of cabinets housing electronic components constrained by space and/or weight severely. With a view at enhancing the heat transfer rates and/or reducing the size of cabinets, the influence that surface radiation exerts upon natural convection should be scrutinized. To this end, the finite volume method is implemented to perform the computational analysis of the above-described problem(s). Numerical results are reported for the local quantities, the velocity and temperature fields encompassing aperture angles φ that extend from 15° to 45° at two extreme Rayleigh numbers, $Ra = 10^3$ and 10^6. Additionally, the two global quantities, the mean convective Nusselt number and the mean radiative Nusselt number are reported in tabulated and graphical forms for the same controlling parameters. Overall, it was found that the competition between surface radiation and natural convection in right-angled triangular cavities filled with air plays a preponderant role. Finally, the analysis culminates with the construction of a comprehensive correlation equation for the total Nusselt number in terms of the controlling parameters which should be useful for engineering analysis and design. This correlation equation will undoubtedly provide a fast evaluation avenue to judge the cavity thermal performance.

1. Introduction

A slim body of literature has been geared toward the quantified competition between natural convection and surface radiation from vertical plates with prescribed hot temperatures to the surrounding air with a goal at invigorating heat removal rates. Early analytic and experimental works on this effort were assembled by Cess [1], Arpaci [2] and Hasegawa et al. [3]. From a historical perspective, the study of natural convection from heated vertical plates has received renewed attention in the last half century due to its growing importance in the electronic industry [4,5].

Although liquid forced convection and boiling offer the highest heat rejection rates from electronic components, air cooling has been, is and will continue to be a widely used technique [6]. In particular, air natural convection is regarded as the most attractive cooling mode when simplicity, economy, reliability and noise become constraint parameters of importance in engineering design. In view of these favorable attributes, research is continually done to gather information about the air cooling limits of electronic components involving natural convection [4–6].

Another configuration of relevance to the electronic industry consists of a heated vertical plate enclosed in a square or rectangular cavity [4,5]. In these standard cavities, the heat exchange by natural convection takes place between the heated vertical plate and the opposite cold plate or between the heated vertical plate and an adjacent

* Corresponding author. Tel.: +34 986 811997; fax: +34 986 811995.
E-mail address: jsieres@uvigo.es (J. Sieres).

0017-9310/$ - see front matter © 2007 Elsevier Ltd. All rights reserved.
doi:10.1016/j.ijheatmasstransfer.2007.07.006

Nomenclature

B	radiosity ($W\,m^{-2}$)
c_p	specific isobaric heat capacity ($kJ\,kg^{-1}\,K^{-1}$)
F_{ij}	view factor from segment i to segment j
g	gravitational acceleration ($m\,s^{-2}$)
G	irradiation ($W\,m^{-2}$)
h	convective coefficient ($W\,m^{-2}\,K^{-1}$)
$\overline{h}$	mean convective coefficient ($W\,m^{-2}\,K^{-1}$)
k	thermal conductivity ($W\,m^{-1}\,K^{-1}$)
L	length of wall (m)
n	total number of boundary differential segments
Nu	Nusselt number, $Nu = h \cdot L/k$
$\overline{Nu}$	mean Nusselt number, $\overline{Nu} = \bar{h} \cdot L/k$
p	pressure (Pa)
q	heat flux ($W\,m^{-2}$)
Ra	Rayleigh number, $Ra = g \cdot \beta \cdot (T_H - T_C) \cdot L_H^3/(\alpha \cdot v)$
s	distance along the wall (m)
T	absolute temperature (K)
u, v	velocity components in the x- and y-directions ($m\,s^{-1}$)
x, y	Cartesian coordinates (m)

Greek symbols

α	thermal diffusivity, $\alpha = k/(\rho \cdot c_p)$ ($m^2\,s^{-1}$)
β	coefficient of volumetric thermal expansion (K^{-1})
δ_{ij}	Kronecker delta
ΔT	prescribed temperature difference ($T_H - T_C$) (K)
ε	total hemispherical emissivity
θ	dimensionless temperature, $(T - T_C)/\Delta T$
μ	dynamic viscosity ($kg\,m^{-1}\,s^{-1}$)
v	kinematic viscosity ($m^2\,s^{-1}$)
ρ	density ($kg\,m^{-3}$)
σ	Stefan–Boltzmann constant ($W\,m^{-2}\,K^{-4}$)
φ	aperture angle (°)
ψ	stream function ($kg\,s^{-1}$)

Subscripts

0	reference value
1	natural convection–radiation coupling
2	pure natural convection
A	adiabatic
C	cold
cri	critical
H	hot
i,j	element indexes
R	radiation
T	total contribution of convection and radiation
V	natural convection

cold plate. State-of-the-art review articles devoted to the theoretical analyses, numerical simulations and experimental observations of natural convection cavity flows can be found in Ostrach [7] and also in the chapters written by Raithby and Hollands [8] and Jaluria [9] in specialized heat transfer handbooks.

Despite that the number of publications on natural convection in square and rectangular cavities is vast [7–9], the number of publications that take into consideration the contribution of surface-to-surface radiation in these closed spaces is scarce, though the impact of surface radiation has been demonstrated to be significant for intermediate-to-high emissivity values of the walls. In fact, the presence of radiation through a transparent gas, such as air, affects the buoyant air velocity and temperature fields in the cavities. This in turn, modifies not only the temperature profiles along the adiabatic wall of the cavities but more importantly the magnitude of the convective coefficients. Laminar natural convection with surface radiation interaction in square cavities filled with air has been studied by Balaji and Venkateshan [10], Akiyama and Chong [11], Ramesh and Venkateshan [12], and Ridouane et al. [13]. All of these authors found an alteration in the mean Nusselt number at the hot wall with increasing wall emissivities. Deviating slightly from the aim of the above references, Bouali et al. [14] examined an inclined rectangular enclosure and detected that surface radiation increases the total Nusselt number, but surprisingly no mention was made about the influence that surface radiation exerts on the convective coefficient.

In this paper, the heat exchange in vertical-oriented right-angled triangular cavities filled with air will be analyzed. These cavities can be envisioned as sliced cavities formed from a standard square cavity wherein buoyant air in conjunction to surface-to-surface radiation transports the heat from the heated vertical wall to the cooled inclined wall. As stated in [4,5], the right-angled triangular cavity configuration finds application in the miniaturization of electronic packaging subjected to space and/or weight constraints. With a view at maximizing heat transfer rates and/or reducing the sizes of electronic cabinets, the relative influence that surface radiation exerts on natural convection should be scrutinized, especially for high wall emissivities. Hence the objective of this paper is to investigate the synergistic effects of wall emissivities, aperture angles and temperature differences on the total heat transfer.

The body of the paper is divided into three sections. The first section describes the problem formulation highlighting the linkage between natural convection and surface radiation. The implementation of the finite volume method in a suitable computational grid is explained in the second

section along with the convergence criterion and the code validation. The third section contains the numerical-determined velocity and temperature fields that lead to the mean convective and mean radiative heat transfer rates at the heated vertical wall. In addition, a comprehensive correlation equation for the efficacious and quick cavity design is included in this section.

2. Problem formulation

2.1. Pure natural convection analysis

The physical system depicted in Fig. 1(a) consists of air confined to a vertically-oriented right-angled triangular cavity made with three impermeable walls. The aperture angle φ identifies the bottom vertex of the triangular cavity. A hot temperature T_H is prescribed at the vertical wall, a cold temperature T_C is prescribed at the inclined wall and the connecting top wall is adiabatic. Owing that the dimension perpendicular to the plane of the diagram is long compared to the cavity height, the air motion is conceived to be two-dimensional. Because the gravitational acceleration g acts parallel to the hot vertical wall, the buoyant air convection may be modeled by the following system of steady conservation equations:

Mass:

$$\frac{\partial u}{\partial x}+\frac{\partial v}{\partial y}=0 \tag{1}$$

Horizontal momentum:

$$\rho\cdot u\cdot\frac{\partial u}{\partial x}+\rho\cdot v\cdot\frac{\partial u}{\partial y}=-\frac{\partial P}{\partial x}+\mu\cdot\frac{\partial^2 u}{\partial x^2}+\mu\cdot\frac{\partial^2 u}{\partial y^2} \tag{2}$$

Vertical momentum:

$$\rho\cdot u\cdot\frac{\partial v}{\partial x}+\rho\cdot v\cdot\frac{\partial v}{\partial y}=-\frac{\partial P}{\partial y}+\mu\cdot\frac{\partial^2 v}{\partial x^2}+\mu\cdot\frac{\partial^2 v}{\partial y^2}+g\cdot(\rho-\rho_0) \tag{3}$$

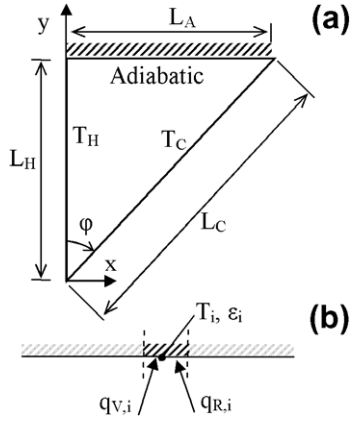

Fig. 1. (a) Sketch of the upright right-angled triangular cavity. (b) The heat balance in a differential segment of the adiabatic top wall.

Energy:

$$u\cdot\frac{\partial T}{\partial x}+v\cdot\frac{\partial T}{\partial y}=\alpha\cdot\frac{\partial^2 T}{\partial x^2}+\alpha\cdot\frac{\partial^2 T}{\partial y^2} \tag{4}$$

The Boussinesq approximation is accounted for in Eq. (3) where ρ_0 denotes a reference density evaluated at the reference temperature $T_0=(T_H+T_C)/2$.

Assuming that the trapped air does not slip at the cavity walls, the velocity boundary conditions are $u=v=0$. The temperature boundary conditions refer to a prescribed high temperature T_H at the vertical wall, a prescribed low temperature T_C at the inclined wall and a null temperature gradient $\frac{\partial T}{\partial y}=0$ at the top adiabatic wall when surface radiation is not taken into account.

2.2. Radiative analysis

When surface radiation transfer is considered in the analysis, the temperature boundary condition at the top adiabatic wall of the triangular cavity must be changed. Thereby, the temperature variation along the adiabatic wall will incorporate the effect of surface radiation on natural convection.

To commence, the energy balance over a differential wall segment i depicted in Fig. 1(b) is stated as

$$q_{V,i}+q_{R,i}=q_{V,i}+G_i-B_i=0 \tag{5}$$

where $q_{V,i}$ is the local convective heat flux that results from applying Fourier's law to the air temperature field $T(x,y)$, $q_{R,i}$ is the local radiative heat flux, G_i is the irradiation falling on the wall segment i and B_i is the radiosity away from the wall surface. The radiosity B_i can be expressed as the sum of the radiation emitted by the wall surface and the irradiated energy reflected by it. Specifically, for an opaque and grey surface, B_i is given by

$$B_i=\varepsilon_i\cdot\sigma\cdot T_i^4+(1-\varepsilon_i)\cdot G_i \tag{6}$$

where ε_i is the total hemispherical emissivity, σ is the Stefan–Boltzmann constant and T_i is the temperature of the wall segment.

Let $A_i\cdot G_i$ designate the amount of irradiating heat transfer falling on the wall segment i, which is the sum of all radiative heat reaching segment i from other surfaces forming the three-wall enclosure. By virtue of the reciprocity rule, the following relation:

$$\sum_{j=1}^{n}\left[\delta_{ij}-(1-\varepsilon_i)\cdot F_{ij}\right]\cdot B_j=\varepsilon_i\cdot\sigma\cdot T_i^4 \tag{7}$$

is obtained where δ_{ij} is the Kronecker delta, n is the total number of segments and F_{ij} is the view factor from segment i to segment j. The numerical values of F_{ij} are determined by Hottel's crossed string rule [15]. The summation term in Eq. (7) is to be taken for all the elements j with which the element i can interact radiatively. Consequently, the

abbreviated Eq. (7) forms a system of algebraic equations accompanying Eq. (5).

3. Numerical computation and validation

The system of partial differential equations (1)–(4), subject to the proper set of boundary conditions is discretized with the finite volume method [16,17]. In the conservation equations, the discretization of the convective term is accomplished by the second-order-accurate QUICK scheme, while the pressure-velocity coupling is handled with the SIMPLE scheme [16]. The velocity field $u(x,y)$, $v(x,y)$ and the temperature field $T(x,y)$ of the moving air depend on the characteristic length L_H, the sweeping aperture angle φ and the imposed temperature difference $T_H - T_C$. If the temperature difference $T_H - T_C$ is merged with the buoyant-to-viscous forces ratio, this operation leads to the height-based Rayleigh number Ra. When surface radiation interacts with natural convection, the two controlling parameters Ra and φ from the natural convection side, plus the hot wall temperature T_H or the cold wall temperature T_C, together with the wall emissivity ε from the radiation side have to be pre-specified.

The energy balance over every segment i along the adiabatic wall expressed by Eq. (5) requires the solution of the system of algebraic equations represented by Eq. (7).

The decision on the grid size was based on sequences of numerical experiments having sizes that range from 10,843 up to 81,698 triangular elements. Special care was taken to increase the triangular element density in vulnerable areas near the walls where steep velocity and temperature gradients would occur inside the hydrodynamic and thermal boundary layers, respectively. A critical case corresponding to the widest $\varphi = 45°$ and the highest $Ra = 10^6$ is selected to perform a sensitivity analysis of the grid. The outcome of this sensitivity analysis is presented in detailed form in Table 1. Herein, important parameters such as the maximum stream function value and the mean Nusselt number $\overline{Nu}$ at the hot wall are reported for the two contrasting situations. One situation involves pure natural convection absent of surface radiation ($\varepsilon = 0$) and the other involves strong convection–radiation interaction which is characterized by $\varepsilon = 1$. The mean Nusselt number values $\overline{Nu}$ reported in Table 1 are within a 0.2% margin. No appreciable differences were found in $\overline{Nu}$ when the grid elements were increased from 40,686 to 81,698, almost double. Hence, the mesh with 40,686 triangular elements was deemed to be adequate and was chosen to carry out the entire numerical calculations.

Table 1
Grid sensitivity analysis for a wide triangular cavity with $\varphi = 45°$ and the highest $Ra = 10^6$

ε	Mesh	ψ_{max}	$\overline{Nu}_{V1}$	$\overline{Nu}_{R1}$	$\overline{Nu}_{T1}$
0	10,843	4.62×10^{-4}	10.34	0	10.34
0	40,686	4.61×10^{-4}	10.32	0	10.32
0	81,698	4.61×10^{-4}	10.32	0	10.32
1	10,843	5.11×10^{-4}	10.99	14.66	25.65
1	40,686	5.10×10^{-4}	10.99	14.66	25.65
1	81,698	5.10×10^{-4}	10.99	14.66	25.65

Local convergence was assessed by monitoring the magnitude of the ultimate quantity, i.e., the mean convective coefficient $\bar{h}$ along the hot vertical and cold vertical walls by setting its variations to less than 10^{-4}. In addition, global convergence was guaranteed by controlling the residuals of the conservation equations to tiny values less than 10^{-5}.

The computational procedure was validated against the experimental observations of Elicer-Cortés and Kim-Son [18]. At the local level, we compared the air temperature profiles at different heights, and at the global level the mean Nusselt numbers $\overline{Nu}$ were contrasted. In the experimental set-up of [18], three slender upright triangular cavities holding aperture angles of $\varphi = 5°$, 10° and 15° were tested. The hot wall temperatures were set at $T_H = 40$, 60, 80 and 100 °C. For the case of a 15° cavity, Fig. 2 illustrates a reasonable parity between the numerically-estimated temperatures and the temperatures measured at three relative heights $y/L_H = 0.1$, 0.58 and 0.99. It is worth pointing out that the lowermost curve for $y/L_H = 0.1$, reveals an overlapping between the numerical predictions and the experimental measurements. It should be pointed out that the numerical temperatures slightly overpredicted the experimental temperatures at the other two relative heights $y/L_H = 0.58$ and 0.99. Invariably, the same patterns prevailed in Fig. 3 for the case of a 10° cavity where the temperature measurements were taken at different relative heights $y/L_H = 0.1$, 0.5 and 0.98. In general, the agreement between the numerical and experimental air temperatures at the three locations is acceptable. Overall, it is observable that the matching between the numerical and the experimental temperatures of [18] tends to improve for the slender upright triangular cavity.

With regards to the mean convective coefficient $\bar{h}$, Table 2 contains a comparison between the computed $\overline{Nu}_{V2}$ and the measured $\overline{Nu}_{V2}$ for the three aperture angles

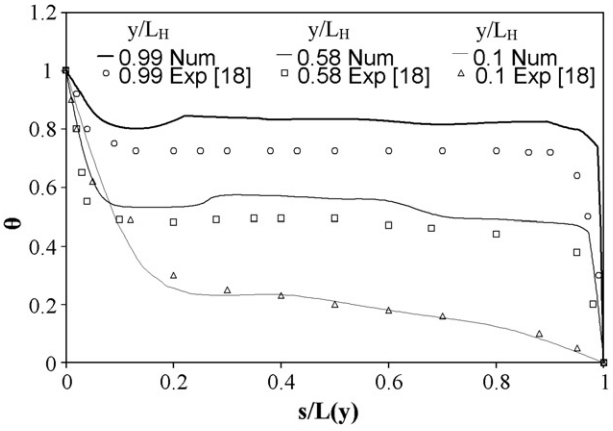

Fig. 2. Comparison between the numerical and experimental temperature profiles at three different elevations inside a 15° triangular cavity.

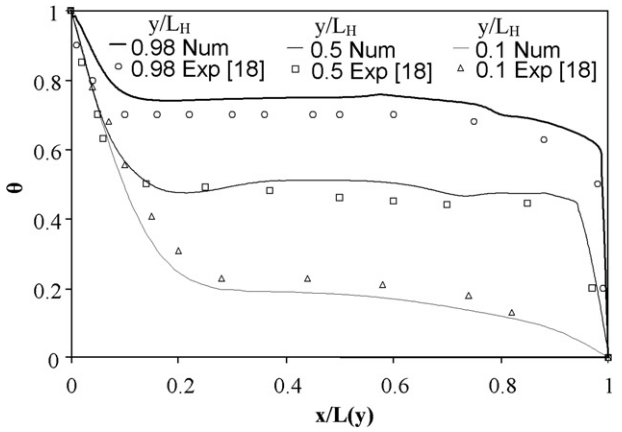

Fig. 3. Comparison between the numerical and experimental temperature profiles at three different elevations inside a 10° triangular cavity.

Table 2
Comparison between the numerical and experimental mean convective Nusselt numbers $\overline{Nu}_{V2}$ at the hot wall for different combinations of φ and T_H

Angle φ	T_H (°C)	$\overline{Nu}_{V2}$ Num.	$\overline{Nu}_{V2}$ Exp.
5°	40	361.9	345.2
	60	374.0	342.1
	80	379.5	348.2
	100	369.3	341.2
10°	40	334.6	300.6
	60	375.4	348.8
	80	368.7	347.3
	100	380.3	343.7
15°	40	354.6	375.1
	60	387.4	392.4
	80	419.7	387.0
	100	420.1	393.2

$\varphi = 5°$, 10° and 15° done by [18]. Because the relative errors for $\overline{Nu}_{V2}$ are aligned within a 11% band, the level of concordance can be considered reasonable.

4. Discussion of results

Air motion was set-up in the right-angled triangular cavities by heating the vertical wall at T_H and cooling the inclined wall at T_C simultaneously, because the top horizontal wall was adiabatic. The aperture angle φ identifying the bottom vertex separating the hot and cold walls takes values of 15°, 30° and 45°. The characteristic length chosen was the height of the hot vertical wall. Accordingly, three cavities were studied having the height-based Rayleigh number that vary from a low $Ra = 10^3$ to a high $Ra = 10^6$. Upon setting the cold wall temperature at $T_C = 287$ K, the temperature difference $\Delta T = T_H - T_C$ between the hot and cold walls spread over a 50 K interval. The wall emissivities ε were allowed to switch from 0 (polished surface) to 1 (black surface).

Numerical solutions dealing with the natural convection–radiation coupling will be compared against the counterpart solutions restricted to pure natural convection. For the sake of brevity, results will be presented only for two triangular cavities, one holding the smallest aperture angle $\varphi = 15°$ and the other the largest angle 45°. The walls are assumed black owing $\varepsilon = 1$; this choice manifests an upper bound for the radiative transfer analysis.

4.1. Velocity and temperature patterns

In Fig. 4, the airflow patterns in terms of the stream function and the temperature are presented at a low $Ra = 10^3$ for the two aperture angles $\varphi = 15°$ and 45° under conditions of pure natural convection ($\varepsilon = 0$). The streamline plots show that both triangular configurations contain a single clockwise rotating vortex, which takes the shape of the entire cavity. The stream function gradient is higher in the 45° cavity than in the 15° cavity, i.e., the streamlines are denser, which means that the velocity values are also higher. With respect to the isotherm curves,

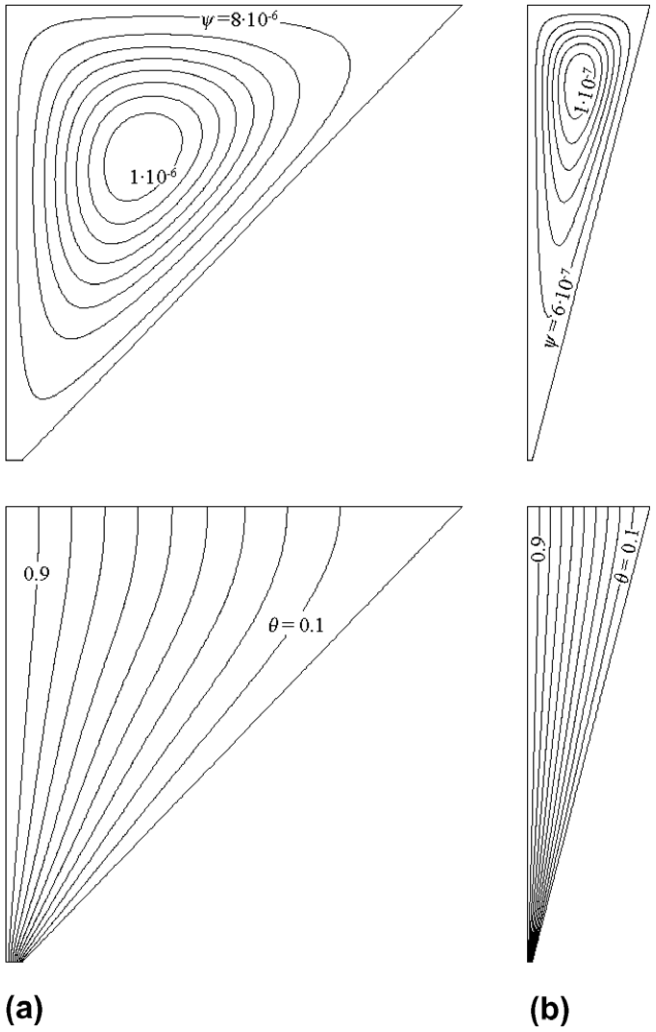

Fig. 4. Streamlines and isotherms related to pure natural convection for $Ra = 10^3$ and two aperture angles φ of (a) 45° and (b) 15°. Other parameters are: $\varepsilon = 0$, $T_C = 287$ K and $\Delta T = 26$ K.

their orientation is vertical denoting that the heat transfer process is overriden by conduction. Moreover, the isotherm lines are somehow distorted, since the warm air moved from the left hot wall to the inclined cold wall, resulting in higher temperatures in the top region of the cavity. It can also be observed that the isotherms are normal to the top wall, in harmony with the imposed adiabatic boundary condition.

Fig. 5 shows the same results that Fig. 4 but considering surface-to-surface radiation ($\varepsilon = 1$). The stream function contours for both configurations are very similar to the ones obtained without the presence of surface radiation. Moreover, the temperature contours are almost identical with the exception that the isotherms on the left are inclined towards the hot wall in the upper region of the cavity. In contrast, the isotherms on the right are inclined towards the cold wall. This phenomenon is due to the nature of the boundary condition on the top adiabatic wall, which implies an outward radiative heat transfer near the hot wall and an inward radiative heat transfer near the cold wall. It seems that the natural convection–radiation interaction is small, especially in the 15° geometry. This statement can be confirmed by contrasting in Table 3 the mean Nusselt number values on the hot wall at $Ra = 10^3$, for pure natural convection ($\overline{Nu}_{V2}$) against the counterpart for natural convection taking into account the new temperature and velocity fields due to radiation interaction ($\overline{Nu}_{V1}$). This comparison brings forward small differences of $\Delta\overline{Nu}_V = 2.8\%$ for the 45° cavity and 0.3% for the 15° cavity when radiation is considered. On the contrary, radiation influences the total heat transfer in a remarkable manner. The equivalent mean Nusselt number due to the radiative heat flux $\overline{Nu}_{R1}$ accounts for $\overline{Nu}_{R1}/\overline{Nu}_{T1} = 11\%$ of the total heat transfer ($\overline{Nu}_{T1}$) for the 15° cavity and grows up to 26% for the 45° cavity and cannot be ignored.

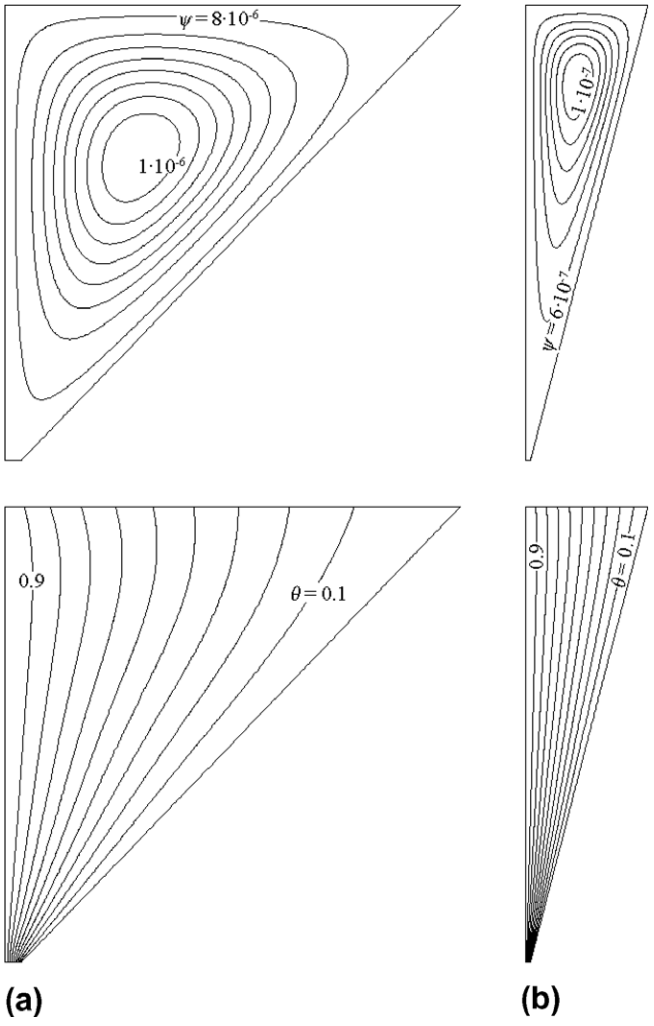

Fig. 5. Streamlines and isotherms related to natural convection-radiation interaction for $Ra = 10^3$ and two aperture angles φ of (a) 45° and (b) 15°. Other parameters are: $\varepsilon = 1$, $T_C = 287$ K and $\Delta T = 26$ K.

Table 3
Mean convective, mean radiative and mean total Nusselt numbers at the hot wall with and without radiation when $\Delta T = 26$ K and $T_C = 287$ K

φ	Ra	$\overline{Nu}_{V2}$	$\overline{Nu}_{V1}$	$\overline{Nu}_{R1}$	$\overline{Nu}_{T1}$	$\Delta\overline{Nu}_V$ (%)	$\frac{\overline{Nu}_{R1}}{\overline{Nu}_{T1}}$ (%)
15°	10^3	13.2	13.3	1.6	14.9	0.3	11
	10^6	15.6	16.0	16.2	32.1	2.2	50
45°	10^3	4.3	4.4	1.5	5.9	2.8	26
	10^6	10.3	11.0	14.7	25.6	6.5	57

Fig. 6 presents the streamlines and isotherms for pure natural convection at the high $Ra = 10^6$. When comparing the 45° configuration in this figure with the one in Fig. 4, it is evident that the vortex has moved down toward the bottom corner of the cavity and the stream function values are increased by two orders of magnitude when compared to the case described by $Ra = 10^3$. This deviation corresponds to higher velocities inside the cavity that translates into the airflow being dominated by natural convection. For the 15° configuration the location of the vortex is not significantly affected, but the magnitude of the stream function has increased in a similar manner. As a consequence, the temperature field $T(x, y)$ is strongly influenced by the velocity field $u(x, y)$, $v(x, y)$ and as a result the isotherms in Fig. 6 are arranged horizontally instead of vertically in the cavity core.

When surface radiation is accounted for by way of $\varepsilon = 1$, the flow patterns are illustrated in Fig. 7. Focusing the attention on the 45° shape, it can be observed that radiation modifies the temperature field. At the bottom of the cavity, the isotherms are analogous to the ones found without radiation interaction. However, when approaching the top adiabatic wall, the effect of radiation heat is noticeable as it tends to cool the hot air layers; this leads to unstable stratification close to the top wall (i.e., cold air over hot air). Surface radiation also touches on the air velocity field inside the closed space, especially near the top. From here, it can be perceived that the streamlines are flattened when compared with their counterparts for pure convection.

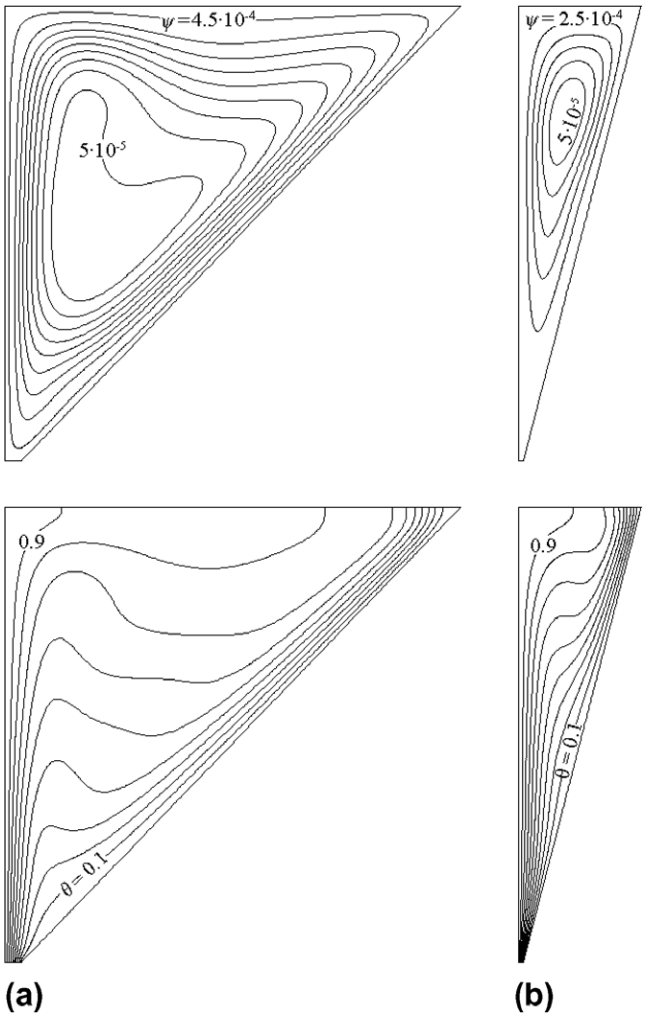

Fig. 6. Streamlines and isotherms related to pure natural convection for $Ra = 10^6$ and two aperture angles φ of (a) 45° and (b) 15°. Other parameters are: $\varepsilon = 0$, $T_C = 287$ K and $\Delta T = 26$ K.

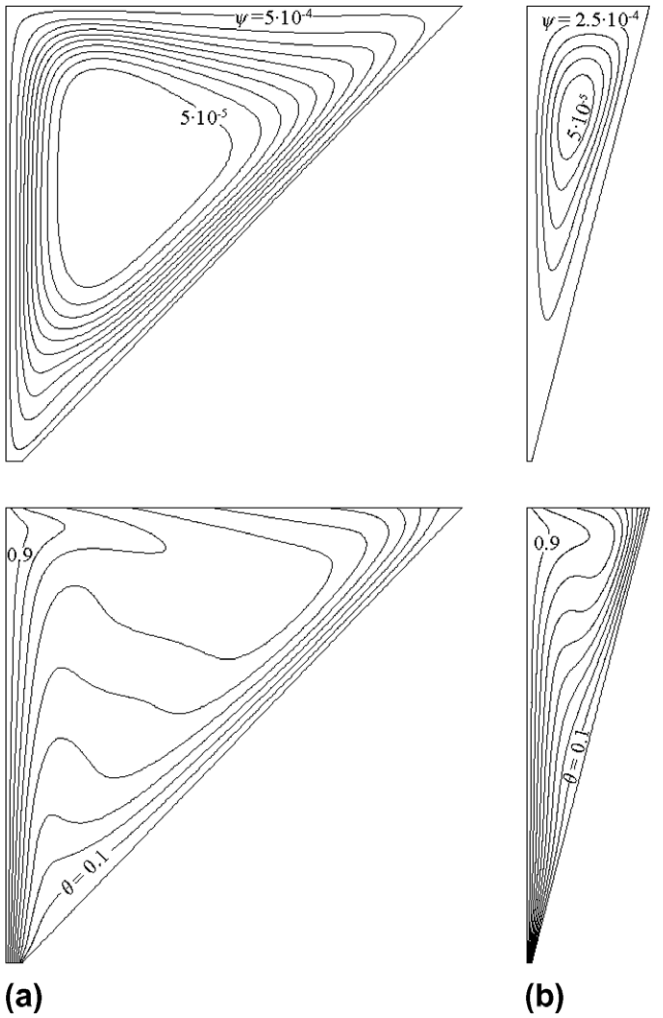

Fig. 7. Streamlines and isotherms related to natural convection-radiation interaction for $Ra = 10^6$ and two aperture angles φ of (a) 45° and (b) 15°. Other parameters are: $\varepsilon = 1$, $T_C = 287$ K and $\Delta T = 26$ K.

Fig. 7 portrays the streamlines and isotherms for the 15° cavity with convection-radiation interaction for the high $Ra = 10^6$. Comparing these results against those for the case of pure natural convection, it is seen that the streamlines are almost identical and that the isotherms are mainly unaffected in the core of the cavity. Towards the top wall, the isotherms are distorted due to the unstable stratification in this region.

In view of the foregoing, it is then concluded that surface radiation has a bearing on the thermal buoyant air inside the two cavities (the slender and the wide) sharing a high $Ra = 10^6$. In this vein, major differences in the mean convective Nusselt number due to the presence of surface radiation are expected. The differences are confirmed from the numbers listed in Table 3, where heat transfer augmentation of the order of 2.2% and 6.5% for the 15° and 45° cavities are achievable when surface radiation is permitted. Moreover, surface radiation elevates the total heat transfer to 50% in the 15° cavity and to 57% in the 45° cavity when paired with a high $Ra = 10^6$.

4.2. Heat transfer features

In order to analyze the heat transfer features of the two dissimilar cavities, the Nusselt numbers are calculated as follows:

$$Nu(s) = \frac{q(s) \cdot L}{k \cdot \Delta T} \tag{8}$$

where s represents the distance along the hot and cold walls measured from the lower vertex and L is the respective wall length. The air thermal conductivity k is evaluated at the reference temperature $T_0 = (T_H + T_C)/2$.

Subsequently, with this information at hand the mean Nusselt number $\overline{Nu}$ can be obtained as

$$\overline{Nu} = \frac{1}{L} \cdot \int_0^L Nu(s) \cdot \mathrm{d}s \tag{9}$$

To assess the effect of surface radiation on the heat transfer performance of natural convection cavities, the distribution of the convective Nusselt number Nu_V and the distribution

of the radiative Nusselt number Nu_R along the three walls are scrutinized for the two limiting conditions: one of pure convection ($\varepsilon = 0$) and the other for the strongest convection–radiation interaction ($\varepsilon = 1$); the two conditions sharing a common $Ra = 10^6$.

In Fig. 8(a), the pure convective Nusselt number along the hot wall Nu_{V2} decreases monotonically from a high value of 26 at the bottom of the vertical hot wall, reaching almost zero at the top of the wall. This trend should be expected, since the separation between the hot and cold walls grows from the bottom to the top of the cavity gradually. With no radiation–convection coupling, the radiative Nusselt number Nu_{R2} increases from a minimum of 7.5 at the bottom of the vertical wall to a maximum of 15 around $y/L_H = 0.09$ and then continues to move with a soft decline with height. This trend responds to the alteration suffered by the view factor F_{ij} connecting the hot wall with the cold wall, which experiences a strong increase from the bottom of the wall to a maximum around $y/L_H = 0.15$. Thereafter, F_{ij} registers a milder decrease with height. From a geometric perspective, the view factors F_{ij} from the hot wall locations to the top adiabatic wall increases monotonically from the bottom of the hot wall to the top, but because the inclined wall temperature is lower the first effect prevails. When radiation is allocated, the convective Nusselt number Nu_{V1} is in general slightly higher than the one for pure convection and poses a similar decreasing tendency to a minimum around $y/L_H = 0.95$. After that, Nu_{V1} is strengthened due to the radiation to the temperature field, which is more pronounced. From the numbers plotted in Fig. 8(a) it can be noticed that the mean convective Nusselt number when coupled with radiation is about 6.5% larger that the one for the pure convection case. On the other hand, the radiative Nusselt number Nu_{R1} is always higher than Nu_{R2}, due to the lower temperatures obtained at the top adiabatic wall; this phenomenon can be seen in Fig. 8(d).

The same two Nusselt numbers along the cold wall are depicted in Fig. 8(b). The pure convective Nusselt number Nu_{V2} descends from a high value at the bottom part to a minimum around a relative distance $s/L_C = 0.1$. After this point is surpassed, an increasing Nusselt number emerged due to the existence of downward air movement along the cold wall, which translates into a state of convection domination over one of conduction domination. Also, at a relative distance along the cold wall $s/L_C = 0.9$, the convective Nusselt number diminishes to zero due to the manifestation of a stagnant zone in the upper right corner of the triangular cavity. When radiation is integrated, the convective Nusselt number Nu_{V1} stays generally lower than the pure convective value Nu_{V2} because radiation tends to cool the hot air layers at the top region of the cavity and softens

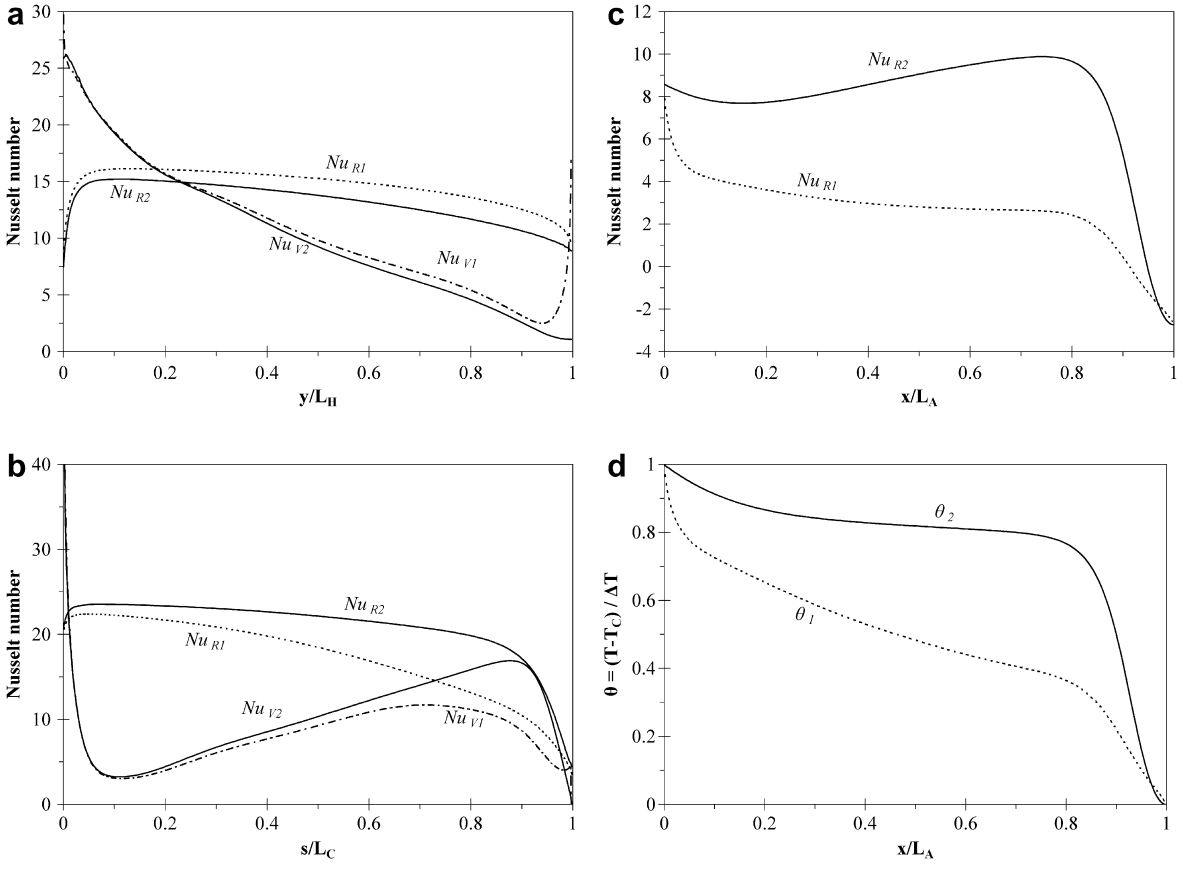

Fig. 8. Local Nusselt numbers along (a) the hot wall, (b) the cold wall and (c) the adiabatic wall. In (d) is the dimensionless temperature along the adiabatic wall for $\varphi = 45°$, $Ra = 10^6$, $\varepsilon = 1$, $T_C = 287$ K and $\Delta T = 26$ K.

the temperature gradients near the cold wall. However, in the upper part of the wall, the opposite effect happens and radiation is responsible for warming the cool layers of air in the vicinity of the adiabatic and cold walls, leading to higher Nusselt numbers than in the case limited to pure convection. A reduction of approximately 19% is palpable for the mean convective Nusselt number when surface radiation is reckoned. If radiation and convection remain uncoupled, the radiative Nusselt number Nu_{R2} takes a nearly flat pattern except in the upper part of the cold wall, where its value decreases sharply. With the incorporation of radiation, the Nusselt values Nu_{R1} are always lower as a direct reaction to the lower temperatures at the top adiabatic wall, as can be seen in Fig. 8(d).

The radiative Nusselt number along the top adiabatic wall is plotted in Fig. 8(c). Also plotted in Fig. 8(d) is the dimensionless temperature along the top adiabatic wall. It was already discussed that for the 45° cavity characterized by $Ra = 10^6$, the overall orientation of the isotherms was horizontal, so a high and uniform temperature profile at the top adiabatic wall is expected and this is confirmed in Fig. 8(d). For almost 80% of the wall length ($x/L_A < 0.8$) the dimensionless temperature stay higher than 0.8 and the radiative Nusselt number Nu_{R2} is high and positive, which means that radiative heat transfer emanates from the surface. For the other locations $x/L_A > 0.8$, the temperature decreases rapidly and so does the radiative heat transfer, the latter becomes negative (radiative heat transfer reaching the wall) for $x/L_A > 0.95$. When convection and radiation interaction is united, a nearly linear temperature profile is obtained. In addition, a constant positive radiative Nusselt number Nu_{R1} surfaces up at the top adiabatic wall, except in the vicinity of the cavity vertices. Opposed to this, the values are highly strengthened resulting in negative values of Nu_{R1} in the colder side of the wall.

The mean convective and mean radiative Nusselt numbers on the hot wall $\overline{Nu}$ are plotted in Fig. 9 as a function of the Rayleigh number for the 15° and 45° closed spaces for fixed T_C, ΔT and ε. Focusing on the 45° configuration in Fig. 9(b), it is clear that the convective Nusselt number $\overline{Nu}_{V2}$ grows with the Rayleigh number from a value of 4.3 at $Ra = 10^3$ to 10.3 for $Ra = 10^6$. When the 45° angle is cut down to 15°, the $\overline{Nu}_{V2}$ increments exhibited remarkable gains. Essentially, this behavior must be attributed to an increased conductive heat transfer related to the small separation between the hot and cold walls. For instance, for the low $Ra = 10^3$, $\overline{Nu}_{V2}$ rises significantly from 4.3 to 13.2, almost a three-fold factor, whereas for $Ra = 10^6$ the $\overline{Nu}_{V2}$ variation moves up from 10.3 to 15.6. Further, it is worth mentioned that $\overline{Nu}_{V2}$ for the 15° cavity stayed nearly constant for Ra up to 10^5. Physically, the attainment of this plateau implies a critical Rayleigh number Ra_{cri} marking the demarcation point between the conduction mode and the onset of the natural convection mode.

The hot convective Nusselt number $\overline{Nu}_{V1}$ allowing for radiation interaction allotted by $\varepsilon = 1$ is also represented in Fig. 9. Here, it is evident that the mean convective Nusselt number increases due to the radiation presence in the whole Ra interval for both the 15° and 45° cavities. The augmentation in the convective Nusselt number is larger at higher Ra and higher aperture angles. In other words, for the 45° cavity the $\overline{Nu}_{V1}$ increment is 2.8% for $Ra = 10^3$ and 6.5% for $Ra = 10^6$. On the contrary, for the 15° cavity these $\overline{Nu}_{V1}$ values descend to a mere 0.3% and 2.2%, so the two curves overlap in Fig. 9(a).

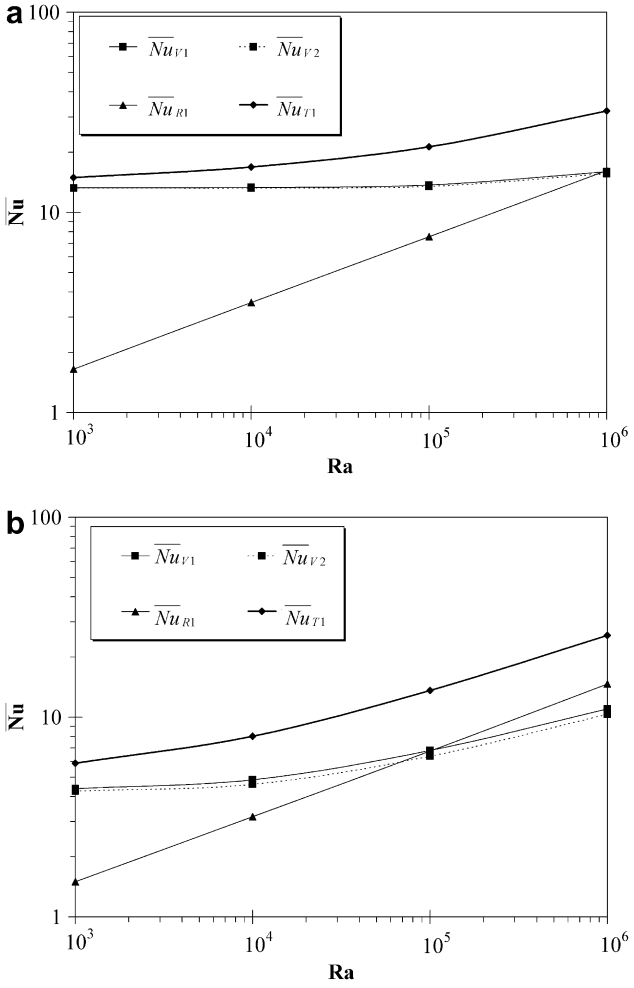

Fig. 9. Variation of the mean Nusselt number with the Rayleigh number at the hot wall for the two aperture angles of (a) 15° and (b) 45°. Other parameters are: $\varepsilon = 1$, $T_C = 287$ K and $\Delta T = 26$ K.

The changes in the mean radiative Nusselt number $\overline{Nu}_{R1}$ with Ra for both cavities are also exposed in Fig. 9. The radiative Nusselt number becomes bigger with Ra and with decreasing aperture angles. Consequently, the total Nusselt number $\overline{Nu}_{T1}$ does the same thing. It is clear from Fig. 9 that the contribution of radiation heat transfer is very important for both cavities sharing the order of magnitude owed by the convective heat transfer. For the 15° cavity, the radiative Nusselt number $\overline{Nu}_{R1}$ is lower than the convective Nusselt number Nu_{V1} for $Ra < 10^6$. This pattern deviates for the 45° cavity wherein the radiative and convective Nusselt numbers are equal at a value around $Ra = 10^5$, but the radiation heat transfer shows signs of domination for higher Ra numbers.

4.3. Uncoupled natural convection and surface radiation

For the sake of simplification, the uncoupled radiative Nusselt $\overline{Nu}_{R2}$ determined from the temperature field emerging from the pure natural convection treatment is compared with the coupled radiative Nusselt $\overline{Nu}_{R1}$ in Fig. 10. This comparison is accompanied by the corresponding value obtained from a simplistic radiative analysis using enclosure theory with isothermal walls; the latter is denoted by $\overline{Nu}_{R,simple}$. In this last case, the radiation heat transfer q_H is calculated through the avenue of the powerful electrical analogy [19]. That is

$$q_H = \frac{\sigma \cdot \left(T_H^4 - T_C^4\right)/A_H}{\frac{1-\varepsilon_H}{\varepsilon_H \cdot A_H} + \frac{1}{\frac{1}{1/(A_H \cdot F_{H-A}) + 1/(A_C \cdot F_{C-A})} + \frac{1}{1/(A_H \cdot F_{H-C})}} + \frac{1-\varepsilon_C}{\varepsilon_C \cdot A_C}} \tag{10}$$

In here, the view factor F_{1-2} refers to an infinitely long enclosure formed by the intersection of three planar walls (1, 2 and 3):

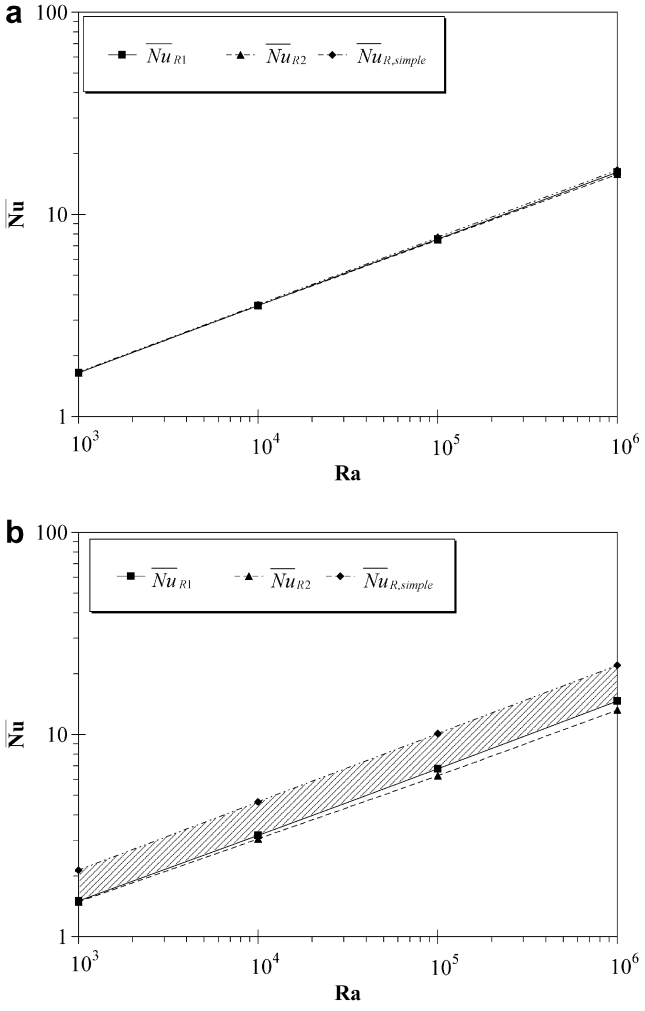

Fig. 10. Variation of the uncoupled and coupled mean radiative Nusselt numbers with the Rayleigh number at the hot wall for two aperture angles of (a) 15° and (b) 45°. Other parameters are: $\varepsilon = 1$, $T_C = 287$ K and $\Delta T = 26$ K.

$$F_{1-2} = \frac{A_1 + A_2 - A_3}{2A_1} \tag{11}$$

which is taken from Siegel and Howell [20].

First, Fig. 10(a) reflects that for the slender 15° cavity regardless of Ra the mean radiation Nusselt number $\overline{Nu}_R$ is invariant with the three computational procedures used. Second, for the 45° cavity, Fig. 10(b) indicates that the mean radiation Nusselt number without coupling $\overline{Nu}_{R2}$ is slightly lower than the $\overline{Nu}_{R1}$ calculated when convection-interaction is accounted for. In numbers at $Ra = 10^3$ the difference is a tiny 1%. However, at $Ra = 10^6$ $\overline{Nu}_{R1} = 14.7$ versus $\overline{Nu}_{R2} = 13.2$; a disparity equivalent to almost 10%. Invariably, when the simple radiative analysis based on isothermal walled-enclosure is brought into the picture, then the mean radiative Nusselt number $\overline{Nu}_{R,simple}$ consistently overpredicts the mean radiation Nusselt number. For instance, the error at $Ra = 10^6$ corresponds to a respectable 50%. A rather interesting feature in Fig. 10 is that the linear variation of $\overline{Nu}_R$ with Ra on log–log coordinates is synonymous with a power law dependence of the form $\overline{Nu}_R = C \cdot Ra^n$ inside the Ra-interval [10^3–10^6].

4.4. Effect of the temperature difference between the hot and cold walls

The effect of the temperature difference ΔT on the heat transfer rates delivered by the triangular cavities is also analyzed. Apart from its primary role in the Rayleigh number, the temperature difference ΔT has an independent influence when radiation is considered. Table 4 displays the impact of ΔT on the mean convective, mean radiative and mean total Nusselt numbers at the hot wall. When the temperature difference ΔT is increased from 10 to 50 K, the convective Nusselt number with radiation interaction $\overline{Nu}_{V1}$ decreases slightly, but the effect is almost unappreciable for the temperature range analyzed. Nevertheless, the radiative Nusselt number reveals an important dependence on the temperature difference and its numerical value decreases with ΔT for a constant Rayleigh number.

Table 4
Effect of the temperature difference ΔT on the mean convective, mean radiative and mean total Nusselt numbers at the hot wall when $\varepsilon = 1$ and $T_C = 287$ K

Fixed parameters	ΔT (K)	$\overline{Nu}_{V2}$	$\overline{Nu}_{V1}$	$\overline{Nu}_{R1}$	$\overline{Nu}_{T1}$
$\varphi = 15°$, $Ra = 10^34$	10	13.2	13.3	2.0	15.3
	26		13.3	1.6	14.9
	50		13.3	0.9	14.2
$\varphi = 15°$, $Ra = 10^6$	10	15.6	16.0	20.1	36.2
	26		16.0	16.2	32.1
	50		16.0	9.1	25.1
$\varphi = 45°$, $Ra = 10^3$	10	4.3	4.4	1.9	6.3
	26		4.4	1.5	5.9
	50		4.4	1.4	5.8
$\varphi = 45°$, $Ra = 10^6$	10	10.3	11.1	18.3	29.4
	26		11.0	14.7	25.6
	50		10.9	13.7	24.6

The discussion of results culminates with a non-linear, multiple regression analysis of the numerical data generated for the three 15°, 30° and 45° cavities, with Rayleigh numbers that range from 10^3 to 10^6 and wall emissivity values varying in 0.2 increments between 0 and 1. Its outcome produced the correlation equation

$$\begin{aligned}\overline{Nu}_{T1} &= \overline{Nu}_{V1} + \overline{Nu}_{R1} \\ &= \left(\frac{3.32}{\varphi} + 5.02 \times 10^{-3} \cdot \varphi^{3/4} \cdot Ra^{0.528}\right) \\ &\quad \cdot \left(1 + 7.69 \times 10^{3} \cdot \varepsilon \cdot \varphi^{1.556} \cdot Ra^{0.210}\right) \\ &\quad + \left[426 - 44.3 \cdot \frac{\sigma \cdot \left(T_H^4 - T_C^4\right)}{\left(T_H - T_C\right)}\right] \times 10^{-3} \cdot \varepsilon^{5/4} \cdot Ra^{1/3}\end{aligned} \tag{12}$$

where the aperture angle φ is expressed in radians and the wall temperatures T_H and T_C in K. Eq. (12) is valid for the three separate intervals $15° \leqslant \varphi \leqslant 45°$, $10^3 \leqslant Ra \leqslant 10^6$, $0 \leqslant \varepsilon \leqslant 1$. The maximum relative error between pairs of the raw data and the predictions is 10% supplying average relative errors that stay below 3%. The proposed correlation equation (12) will find application in engineering analysis and design providing a fast evaluation for cavity thermal performance.

5. Conclusions

For the first time, the problem of natural convection and its interaction with surface radiation has been solved for a sub-class of right-angled triangular cavities filled with air. Several combinations of the height-based Rayleigh number Ra, the aperture angle φ, wall emissivities ε and prescribed temperature difference ΔT were studied with the finite volume method.

The numerical results showed that the mean convective Nusselt number at the hot wall increases when the height-based Rayleigh number increases. In contrast, the mean convective Nusselt number at the hot wall increases when the aperture angle φ decreases. Owing that surface radiation alters the air velocity and temperature fields inside the cavity, this leads to an elevation in the convective Nusselt number on the hot wall. Moreover, the contribution of the radiative heat flux to the total heat flux turns out to be more significant for high Ra. The radiative Nusselt number becomes bigger with increasing Rayleigh numbers and decreasing aperture angles. The temperature difference between the hot and cold walls ΔT seems to have an independent influence and it is evident that for a constant Rayleigh number the radiative Nusselt number decreases with ΔT. When calculating the radiative Nusselt number, the numerical results showed that their values considering natural convection–radiation interaction are higher than when no interaction is considered. However, the results are lower than the uncoupled solution obtained from a simplistic radiative analysis using enclosure theory with constant temperature surfaces, leading to important errors especially for increasing aperture angles.

For real engineering applications, a comprehensive correlation equation is indispensable. Accordingly, a correlation equation has been reported which may be useful for efficacious cavity design.

Acknowledgement

Jaime Sieres thanks "Xunta de Galicia" for supporting his stay at the Department of Mechanical Engineering of the University of Vermont.

References

[1] R.D. Cess, The interaction of thermal radiation with free convection heat transfer, Int. J. Heat Mass Transfer 9 (1966) 1269–1277.
[2] V.S. Arpaci, Effect of thermal radiation on the laminar free convection from a heated vertical plate, Int. J. Heat Mass Transfer 11 (1968) 871–881.
[3] S. Hasegawa, R. Echigo, K. Fukuda, Analytical and experimental studies on simultaneous radiative and free convective heat transfer along a vertical plate, Proc. Jpn. Soc. Mech. Eng. 38 (1972) 2873–2882.
[4] R.E. Simons, V.W. Antonnetti, W. Nakayawa, S. Oktay, Heat transfer in electronic packages, in: R.R. Tummala, E.J. Rymaszewski, A.G. Klopfenstein (Eds.), Microelectronics Packaging Handbook, second ed., Chapman and Hall, New York, 1997, pp. 1-315–1-403.
[5] A. Bar-Cohen, A.A. Watwe, R.S. Prasher, Heat transfer in electronic equipment, in: A. Bejan, A.D. Kraus (Eds.), Heat Transfer Handbook, Wiley, New York, 2003 (Chapter 13).
[6] R.C. Chu, The challenges of electronic cooling: past current and future, J. Electron. Packaging 126 (2004) 491–500.
[7] S. Ostrach, Natural convection in enclosures, J. Heat Transfer 110 (1988) 1175–1190.
[8] G.D. Raithby, K.G.T. Hollands, Natural convection, in: W.M. Rohsenow, J.P. Hartnett, Y.I. Cho (Eds.), Handbook of Heat Transfer, third ed., McGraw-Hill, New York, 1998 (Chapter 4).
[9] Y. Jaluria, Natural convection, in: A. Bejan, A.D. Kraus (Eds.), Heat Transfer Handbook, Wiley, New York, 2003 (Chapter 7).
[10] C. Balaji, S.P. Venkateshan, Interaction of surface radiation with free convection in a square cavity, Int. J. Heat Fluid Flow 3 (1993) 260–267.
[11] M. Akiyama, Q.P. Chong, Numerical analysis of natural convection with surface radiation in a square enclosure, Numer. Heat Transfer Part A 31 (1997) 419–433.
[12] N. Ramesh, S.P. Venkateshan, Effect of surface radiation on natural convection in a square enclosure, J. Thermophys. Heat Transfer 13 (1999) 299–301.
[13] E.H. Ridouane, M. Hasnaoui, A. Amahmid, A. Raji, Interaction between natural convection and radiation in a square cavity heated from below, Numer. Heat Transfer Part A 45 (2004) 289–311.
[14] H. Bouali, A. Mezrhab, H. Amaoui, M. Bouzidi, Radiation–natural convection heat transfer in an inclined rectangular enclosure, Int. J. Therm. Sci. 45 (2006) 553–566.
[15] H.C. Hottel, A.F. Sarofim, Radiative Heat Transfer, McGraw-Hill, New York, 1967.
[16] S.V. Patankar, Numerical Heat Transfer and Fluid Flow, Hemisphere, Washington, DC, 1980.
[17] H.K. Versteeg, W. Malalasekera, An Introduction to Computational Fluid Dynamics, second ed., Prentice Hall, Harlow, 2007.
[18] J.C. Elicer-Cortés, D. Kim-Son, Natural convection in a dihedral cavity: influence of the angle and the temperature of the walls on the mean thermal field, Exp. Heat Transfer 6 (1993) 205–213.
[19] J.H. Lienhard IV, J.H. Lienhard V, A Heat Transfer Textbook, third ed., Phlogiston Press, Cambridge, MA, 2006.
[20] R. Siegel, J.R. Howell, Thermal Radiation Heat Transfer, fourth ed., Taylor and Francis, Hemisphere, Washington, DC, 2001.